

Redox Potentials of Uranyl Ions in Macrocyclic Complexes: Quantifying the Role of Counter-Ions

Mahesh Sundararajan*

Cite This: *ACS Omega* 2023, 8, 18041–18046

Read Online

ACCESS |



Metrics & More

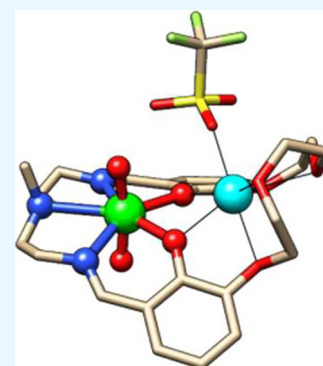


Article Recommendations



Supporting Information

ABSTRACT: Several uranyl ions strapped with Schiff-base ligands in the presence of redox-innocent metal ions are synthesized, and their reduction potentials are recently estimated. The change in Lewis acidity of the redox-innocent metal ions contributes to ~ 60 mV/ pK_a unit quantified which is intriguing. Upon increasing the Lewis acidity of metal ions, the number of triflate molecules found near the metal ions also increases whose contributions toward the redox potentials remain poorly understood and not quantified until now. Most importantly, to ease the computational burden, triflate anions are often neglected in quantum chemical models due to their larger size and weak coordination to metal ions. Herein, we have quantified and dissected the individual contributions that arise alone from Lewis acid metal ions and from triflate anions with electronic structure calculations. The triflate anion contributions are large, in particular, for divalent and trivalent anions that cannot be neglected. It was presumed to be innocent, but we here show that they can contribute more than 50% to the predicted redox potentials, suggesting that their vital role in the overall reduction processes cannot be neglected.



INTRODUCTION

Nuclear energy is an indispensable energy resource for the ongoing energy demand, but efficient waste management processes of the spent nuclear fuel pose a major environmental challenge.^{1,2} Uranyl ions, $[UO_2]^{2+}$, possess high aqueous solubility, and toxicity is a major problem that can contaminate water resources.³ Anaerobic bacteria containing cytochrome *c7* proteins able to convert toxic U(VI) to nontoxic and insoluble U(IV) form through reduction and disproportionation mechanisms.^{4,5} In this direction, several macrocyclic ligands bearing N- and O-donor ligands are synthesized that can selectively extract uranyl ions in the presence of other interfering ions.^{6–10}

Lewis acidic metal ions are often used to stabilize the reactive intermediates of high valent metal ions and metalloenzymes.^{11–15} Their nearby presence is presumed to tune the redox potentials of catalytically active intermediates.^{16–18} Recently, the Blakemore group elegantly designed a Schiff base ligand with an extended crown ether that can complex both uranyl ions and Lewis acid metal ions. They reported the X-ray crystal structures and one-electron reduction potentials of several U(VI) complexes bound near the Schiff base site anchored by different redox innocent metal ions (M^{n+}) strapped to the crown ether as shown in Figure 1. They proposed that redox-inactive metal ions modulate the redox potentials of uranyl complexes. The change in Lewis acidities of the metal ions contributes to 60 mV/ pK_a unit which is intriguing. The X-ray structures clearly show that triflate (OTf^-) counter-anions are bound to M^{n+} , but their contribution to the overall redox potentials is not quantified.

To appreciate the Lewis acid contributions to redox potentials of uranyl complexes, first it is mandatory to quantify the redox

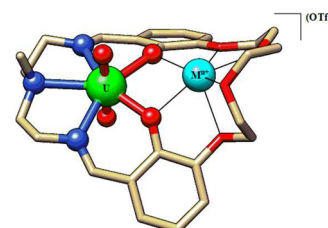


Figure 1. $[UO_2]^{2+}$ ion bound to a Schiff base ligand. Green, blue, red, cyan, and gray indicate U, N, O, Lewis acid metal ion, and C, respectively. Hydrogens are removed for clarity.

potentials that arise from Lewis acids without OTf^- and with Lewis acids and OTf^- counter-anions. Finally, the reduction potential of Y^{3+} bound uranyl -1.29 V is lower by 110 mV compared to those of Ca^{2+} bound species, whereas the corresponding pK_a of the former is 4.6 units larger than that of the latter ion.

The X-ray structures of uranyl(VI) species with the counter-ions are known,¹⁹ whereas the corresponding (V) species are lacking. Thus, to what extent the geometries are varied upon reduction is unclear from the experiments that warrant a need for a quantum chemical study. Ghosh and co-workers²⁰ noted

Received: February 24, 2023

Accepted: April 27, 2023

Published: May 10, 2023



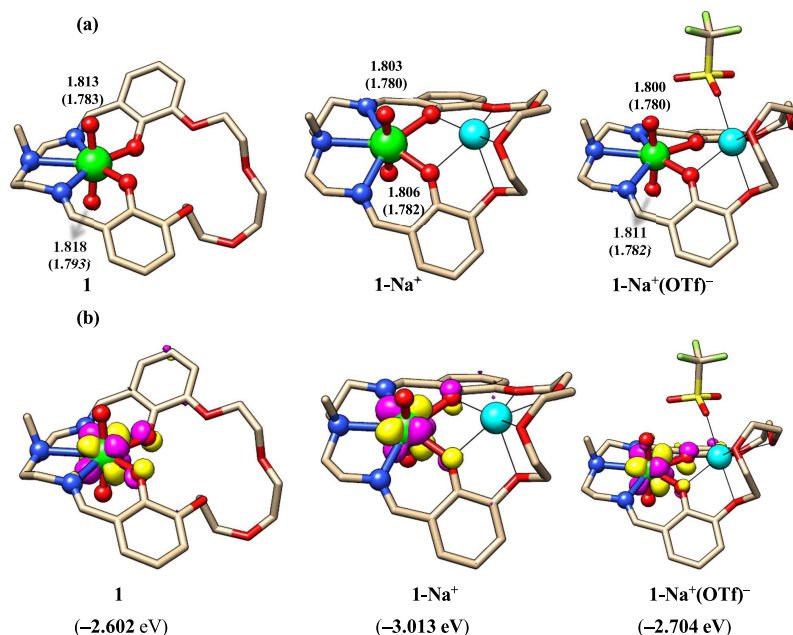


Figure 2. (a) Optimized structures (in Å) and (b) LUMOs of **1**, **1-Na⁺**, and **1-Na⁺(OTf)⁻** (contour value = 0.04 a.u.). Values in parenthesis are experimental bond lengths.

that Lewis acid presence lowers the redox active molecular orbital (RAMO) of uranyl(VI) species which in turn reduces the redox potentials, whereas the corresponding U(V) species are never computed. It should be noted that for d-block elements, a systematic density functional theory (DFT)-based protocol to compute the redox potentials is reported.^{21–24}

In this paper, we have systematically dissected and quantified the crucial role of redox-inactive M^{n+} and OTf^- ions through electronic structure calculations. Apart from a few actinide complexes,^{19–27} the redox potentials were never computed at the molecular level that reveals the complexity of the systems such as the importance of counter-ions,^{28,29} solvation, and relativistic effects. A correlation between the pK_a , vibrational frequencies against the oxidation state, and the redox potentials is quantified through our DFT calculations.

RESULTS AND DISCUSSION

The uranyl bound Schiff base complex is labeled as **1**, whereas that with different counter-cations is labeled as **1-Mⁿ⁺**, where M^{n+} denotes K^+ , Na^+ , Ca^{2+} , and Y^{3+} ions. In the reported X-ray structures, one to three OTf^- anions are found to neutralize the charges carried by the redox innocent metal ions. These species are labeled as **1-Mⁿ⁺(OTf)ⁿ⁻**. The representative optimized structures of **1**, **1-Na⁺**, and **1-Na⁺(OTf)⁻** are shown in Figure 2. The optimized structures of all species **1**, **1-Mⁿ⁺**, and **1-Mⁿ⁺(OTf)ⁿ⁻** in VI and V oxidation states are shown in Figures S1 to S4, and the optimized structural parameters are shown in Table S1.

The most notable geometric parameter to be analyzed is the axial $U=O$ bond length. The computed $U=O$ bond lengths in **1** is 1.81 Å in close agreement with the X-ray value of 1.79 Å. Upon adding redox innocent metal ion in near vicinity with increasing Lewis acidity, the $U=O$ bond length decreases from 1.81 to 1.79 Å in line with the experimental variation from 1.79 to 1.77 Å. This 0.02 Å change in the bond length although minimal is strongly reflected in the asymmetric stretching of the $U=O$ bond as shown in Figure 3. The ν_{asym} of the $U=O$ bond is 872 and 923 cm^{-1} for **1** and **1-Y³⁺** species, respectively. An

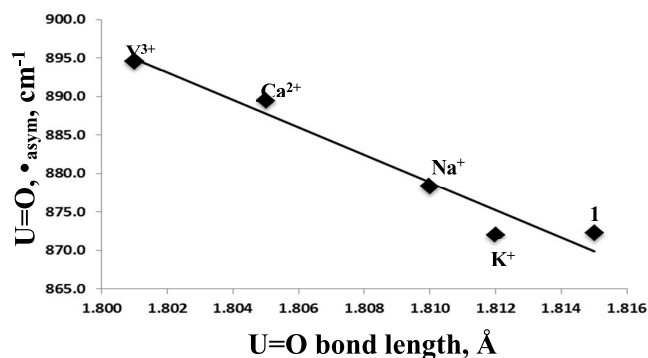


Figure 3. Computed vibrational frequencies, cm^{-1} .

increment of 10 cm^{-1} per metal ion with increasing Lewis acidity is predicted from our calculations that provides new insights on the geometric structures of Uranyl complexes.

In the X-ray structures of **1-Mⁿ⁺(OTf)ⁿ⁻** species, we note that several OTf^- molecules are found in near vicinity to the redox-innocent metal ions. For Na^+ and K^+ ions, one OTf^- molecule is noted, whereas for Ca^{2+} and Y^{3+} ions, one OTf^- and two OTf^- ions are bound to the Lewis acids, whereas one OTf^- is not bound to them due to steric hindrance. Instead, solvent molecules such as methanol and acetonitrile are bound to the redox innocent metal ions. The unbound OTf^- hydrogen bonded with the solvent molecules should be incorporated in the calculations for reliable predictions of redox properties. We have retained these solvent molecules and OTf^- anions in our calculations and the optimized structures are shown in the SI.

The presence of OTf^- anions modifies the geometric parameters around the Lewis acid and the uranyl moiety in all complexes. Particularly, we note that effects are larger for Ca^{2+} and Y^{3+} analogs. In **1-Mⁿ⁺OTfⁿ⁻** species, the shortening of the $U=O$ bond length with varying M^{n+} is noted as compared to those of geometries with **1-Mⁿ⁺** species. However, a small reduction of $U=O$ bond length of about 0.01 Å is noted.

The geometries of Ca^{2+} and Y^{3+} species are further scrutinized in the presence of triflates only by removing the bound solvent molecules. The optimized structures of hexa- and pentavalent oxidation states of uranyl are shown in Figure S5. Compared to the X-ray structures, the triflate alone bound species are somewhat different to those of the mixed solvent and counter-ions. For instance, the $\text{U}-\text{Ca}^{2+}$ and $\text{U}-\text{Y}^{3+}$ distances are now shorter by more than 0.1 Å compared to the X-ray structures. Similarly, the OTf^- anion binds Ca^{2+} ion through the bidentate coordination mode, whereas, in the X-ray structures, they are monodentate. For $1-\text{Y}^{3+}(\text{OTf})_3^-$ species, we always note that one of the OTf^- anion disassociates from the Lewis acid. Thus, the OTf^- only bound structures of Ca^{2+} and Y^{3+} are also energetically high compared to those mixed solvent-counter-anion bound species by more than 23.0 and 18.6 kcal/mol. Thus, the role of solvent molecules is particularly important for highly charged Lewis acids.

In terms of asymmetric $\text{U}=\text{O}$ stretching vibrational frequencies, the computed values increase by only 22 cm^{-1} from **1** to $1-\text{Y}^{3+}(\text{OTf})^-$. Overall, the computed geometric parameters of all species are in line with the X-ray data only in the presence of both Lewis acid and OTf^- anions. Although this may seem obvious, the presence of counter-ions has a pronounced effect on the redox properties that will be discussed below (*vide infra*).

Upon reduction, the axial $\text{U}=\text{O}$ bond length increases by $\sim 0.03\text{ Å}$ for all species as shown in Table S1, Figures S2 and S4. Correspondingly, the $\text{U}(\text{V})\cdots\text{M}^{n+}$ distance decreases due to the increased electrostatic interaction between the Lewis acid metal ion and the reduced uranyl(V) moiety. This can be easily understood as follows: Upon reducing $\text{U}(\text{VI})$ species, the gained negative charge on uranyl is stabilized by charge transfer from Lewis acids metal ions.

The added electron goes to the lowest unoccupied molecular orbital (LUMO) of $\text{U}(\text{VI})$ that has a dominant f-character indicating a metal based reduction, and the Schiff base ligand is redox innocent. The presence of M^{n+} and OTf^- ions has a dominant effect on the RAMO that is primarily the LUMO of an f-orbital as shown in Figure 2b. For instance, the RAMO of $1-\text{Na}^+$ and $1-\text{Na}^+(\text{OTf})^-$ is stabilized by -0.41 and -0.10 eV compared to **1**. Upon increasing the Lewis acidities of M^{n+} , the RAMOs are further stabilized as shown in Figure 4.

The above figure illustrates the presence of Lewis acid metal ions overstabilizes the RAMO drastically from -2.60 eV for **1** to -4.10 eV for $1-\text{Y}^{3+}$. Thus, the vicinity of Lewis acid metal ions changes the relative RAMO energies by 1.50 eV , whereas the experimentally observed reduction potential varies by only

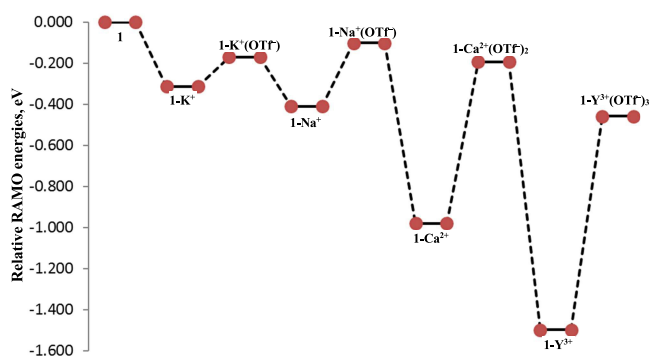


Figure 4. Change in relative RAMO energies (in eV) with increasing Lewis acidities and counter-anions.

-0.36 V . In the presence of OTf^- anions, the RAMO energies vary by only 0.49 eV that is in line with the experimental data.

We have computed the binding affinities of OTf^- anions to $1-\text{M}^{n+}$ species as shown in Table S2. As expected, the binding of OTf^- anions is highest for $1-\text{Y}^{3+}$ and least for $1-\text{Na}^+$ for both hexavalent and pentavalent oxidation states. These variations clearly indicate the importance of incorporating OTf^- anion for the accurate prediction of redox potential. Hence, direct computation of reduction potentials of all five species with and without the OTf^- ions will directly reveal the M^{n+} and OTf^- contributions to the overall redox potential.

In Table 1, we show the computed reduction potentials of all five species in the presence of M^{n+} and OTf^- and compared them against the experimental data (standard, Fc/Fc^+). Compared to experimental data of -1.54 V , our predicted redox potential of **1** is slightly underestimated by just 21 mV that is typical with computational methods. The presence of Lewis acid metal ions alone drastically increases the redox potential from -1.26 V for $1-\text{K}^+$ to -0.25 V for $1-\text{Y}^{3+}$. This is not surprising due to their relative RAMO stability as indicated in Figure 4. The reported experimental redox potential is for the whole species that includes triflate anions and not just for the Lewis acid. The computed value for **1** is within 21 mV , whereas for the other species, the computed errors are huge (by more than 1000 mV for $1-\text{Y}^{3+}$ ion) which indicates some important contributions are missing in this model. The increased stabilization can be attributed to the large stabilization of RAMO as shown in Figure 4.

The presence of OTf^- bound to M^{n+} stabilizes the RAMO to a lesser extent compared to M^{n+} and thus the predicted redox potential varies from -1.39 to -1.10 V only. Our computed values for all four species are in excellent agreement with the experimental values of -1.36 to -1.29 V . Unlike $1-\text{M}^{n+}$ species, where the RAMO's are overstabilized, the incorporation of OTf^- anions stabilizes the LUMO of **1** but only moderately leads to the accurate prediction of redox potential.

For all five species, our computed redox potentials are well reproduced by our calculations only in the presence of M^{n+} supported by OTf^- . To quantify M^{n+} and OTf^- ions, we have computed the percentage error of the computed redox potentials with respect to the experimental data as shown in Table 1. For K^+ and Na^+ ions, the computed redox potential is overestimated by 7 and 12%, whereas in the presence of both metal ions and a triflate anion, the computed potential are within 2% to the experimental value. Thus, the effect of triflate anion contributes to 5 and 10% for K^+ and Na^+ . For the divalent Ca^{2+} ion bound near the uranyl, the redox potential is overestimated by 41%, whereas the presence of two triflate anions brings back the redox potential within 35 mV to the experimental value. Thus, the overall contribution arising from two OTf^- is $\sim 38\%$.

Experiments were carried on two trivalent ions, namely, Nd^{3+} and Y^{3+} ion and their redox potentials are estimated to be -0.98 and -1.29 V , respectively, whereas their corresponding pK_a of the two ions is similar ($\sim 8\text{ pK}_a$ units). In fact, the experimental potential of Y^{3+} is lower than the Ca^{2+} by 0.11 V and for Nd^{3+} ion, the value is higher by 0.2 V that is inline with the experimental pK_a trends as shown in Figure 5. Our computed redox potential in the presence of Y^{3+} ion and with both counter-ions is -0.29 and -1.10 V . Our computed values have an error of more than 1 and 0.69 V with respect to Y^{3+} and Nd^{3+} ion, whereas upon adding three OTf^- ions, the computed values are overestimated by 0.2 V and underestimated by 0.1 V ,

Table 1. Computed Redox Potential (ΔE_0), V, Percentage Error in Redox Potential without and with Counter-Ions, and the Computed DFT Error against the Experimental Value in mV

	computed ΔE_0		expt, ΔE_0	percentage contribution of counter-ions			computed error from expt, ΔE_0	
	M^{n+}	M^{n+} & OTf^-		M^{n+}	M^{n+} & OTf^-	OTf^-	M^{n+}	M^{n+} & OTf^-
1	-1.561		-1.54	0			-21	
1-K⁺	-1.261	-1.391	-1.36	7.3%	2.3%	5.0%	99	-31
1-Na⁺	-1.159	-1.293	-1.32	12.2%	2.0%	10.2%	161	27
1-Ca²⁺	-0.701	-1.215	-1.18	40.6%	3.0%	37.6%	479	-35
1-Y³⁺	-0.288	-1.099	-1.29 (-0.98) ^a	77.7% (29.9%)	14.8% (12.1%)	62.9% (17.8%)	1002 (692)	+191 (-119)

^aValues in parentheses are for the corresponding uranyl complex with Nd^{3+} complexes as redox inactive metal ion.

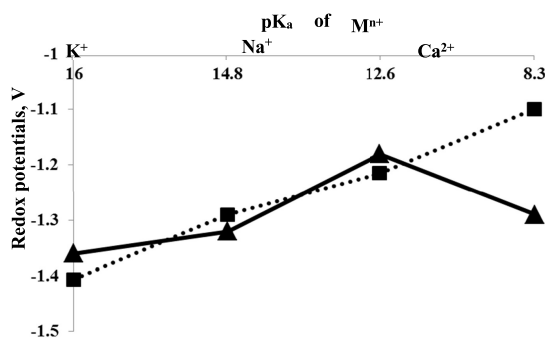


Figure 5. Relationship between pK_a and redox potentials (in V). Dotted and straight lines indicate computed and experimental values, respectively.

respectively. Thus, OTf^- alone contributes more than 50% to the net redox potential that is not negligible.

It should be noted that unlike the computation, it is difficult to partition the redox potential that arises alone from Lewis acid and from both Lewis acids and counter-ions. The experimental pK_a 's of Ca^{2+} and Y^{3+} ions are 12.6 and 8.3 units, whereas the experimental redox potentials are -1.18 and -1.29 V as shown in Figure 5. The redox potential of **1-Y³⁺** ion should be larger than that of the corresponding **1-Ca²⁺** ion, whereas the estimated values are -1.29 and -1.18 V for **1-Y³⁺** and **1-Ca²⁺** that do not correlate with the pK_a trends. Based on DFT calculations, we predicted -1.21 and -1.10 V for **1-Ca²⁺** and **1-Y³⁺**, respectively, that nicely matches with the RAMO energies and pK_a 's of Ca^{2+} and Y^{3+} (or Nd^{3+}) ions. To further justify our claim, the Blakemore group²⁸ reported the M^{n+} modulation of the redox potential of Ni(II/I) complexes with the identical Schiff base ligand framework. The estimated redox potentials of **Ni-Y³⁺** and **Ni-Ca²⁺** complexes are -1.22 and -1.42 V with the Fc/Fc^+ reference electrode which nicely matches with the pK_a trends. Similarly, Reath et al. also noticed that pK_a and redox potentials vary systematically in Cobalt Schiff base complexes.²⁹

Finally, the Mulliken charge on U decreases in the presence of Lewis acid and counter-ions. The net charge on U decreases from $1.014 e^-$ in **1** to $0.911 e^-$ in **1-Mⁿ⁺(OTf⁻)_n**. These variations clearly indicate that the counter ions stabilizes the uranyl ion as shown Table S3 and Figure S6.

CONCLUSIONS

Several reactions including small molecule activations are dictated by their redox potentials that are difficult to predict at the molecular level. For a heavy metal ion like uranyl, it is even more challenging due to the lesser known speciation of U(V) species. In this paper, we report the first and accurate prediction of redox potentials of five uranyl complexes and quantified the contributions that arise from M^{n+} and OTf^- ions. Our predicted

redox potentials have error bars within ± 35 mV for **1**, **1-K⁺**, **1-Na⁺**, and **1-Ca²⁺** species, and ± 120 mV for **1-Y³⁺** ion is the best that has been computed so far. As OTf^- anions are often used to stabilize several reactive intermediates, its contribution just as a cation neutralizer should be revisited in the future.

EXPERIMENTAL SECTION

We have constructed the geometric models of the five uranyl species derived from the reported X-ray structures.¹⁹ We have carried out two sets of calculations. In the first set, all counter-ions and solvents are removed, whereas, in the second set, all counter-ions are retained. Both geometry optimizations and vibrational frequency computations are carried out using DFT.³⁰ DFT calculations were carried out as implemented in the TURBOMOLE 7.2 version of *ab initio* quantum chemistry program.³¹ Geometry optimizations were performed with BP86 functional^{32,33} including Grimme's D3 dispersion correction³⁴ with Becke-Johnson damping factor (D3-BJ).³⁵ All atoms except U are represented using the *def2-TZVP* basis set.³⁶ For U, a *def-TZVP* basis set and the core electrons are treated with a small core pseudopotential ($Z = 60$). The calculations are accelerated using a resolution of identity (RI) approximation by incorporating the corresponding auxiliary basis set. Analytical vibrational frequencies within the harmonic approximation were computed with the abovementioned basis sets to confirm proper convergence to well-defined minima. Standard approximation was used to obtain zero-point vibrational energy and entropy corrections. We obtained solvation energies using the optimized gas-phase structures from the COSMO solvation model with dielectric constant $\epsilon = 35.46$ (acetonitrile) using the default radii. Single point calculations are carried out with the M06 functional.

The energy components have been computed with the following protocol. The free energy in solution phase $G(\text{sol})$ has been calculated as follows:

$$G(\text{sol}) = G(\text{gas}) + G^{\text{solv}} \quad (1)$$

$$G(\text{gas}) = H(\text{gas}) - TS(\text{gas}) \quad (2)$$

$$H(\text{gas}) = E(\text{SCF}) + \text{ZPE} \quad (3)$$

$$\Delta G(\text{sol}) = \sum G(\text{sol}) \text{ for U(V)} - \sum G(\text{sol}) \text{ for U(VI)} \quad (4)$$

$G(\text{gas})$ is the free energy in the gas phase; G^{solv} is the free energy of solvation as computed using the continuum solvation model; $H(\text{gas})$ is the enthalpy in the gas phase; T is the temperature (298.15 K); $S(\text{gas})$ is the entropy in the gas phase; $E(\text{SCF})$ is the self-consistent field energy, i.e., "raw" electronic energy as computed from the SCF procedure and ZPE is the zero-point energy. Note that by entropy here we refer specifically to the

vibrational/rotational/translational entropy of the solute(s); the entropy of the solvent is incorporated implicitly in the continuum solvation model.

We have earlier used this computational strategy for several systems and their agreement with experiments is satisfactory.^{37,38} Chimera 1.12c³⁹ is used to plot the molecular orbitals (iso value of 0.05).

Redox potentials are calculated using the following equations, reference electrode:

$$\Delta G_{\text{soln}}(\text{Fc}) = \Delta G_{\text{soln}}([\text{Fc}] - [\text{Fc}^+]) \quad (5)$$

Uranyl Redox Potential:

$$\Delta G_{\text{soln}}(\mathbf{1}) = \Delta G_{\text{soln}}[\mathbf{1}]^- - \Delta G_{\text{soln}}[\mathbf{1}] \quad (6)$$

$$\text{Raw } E^\circ = \Delta G_{\text{soln}}(\text{Fc}) - \Delta G_{\text{soln}}(\mathbf{1}) \quad (7)$$

$$\text{Corrected } E^\circ \text{ for multiplet effects} = \text{Raw } E^\circ - 0.31 \quad (8)$$

Based on multireference calculations, Hay and co-workers reported the multiplet effects of U(VI/V) species to be -0.31 eV.^{22,40} We have used this value to correct the raw redox potential. In Table S4, we have shown the redox potentials of **1** with different density functionals that are commonly used. Among the five DFs, the M06 functional predicted a value of -1.56 V close to the experimental estimate of -1.54 V within 100 mV. We have earlier shown that the M06 functional predicts vertical and adiabatic detachment energies of uranyl complexes in close agreement with electron spray ionization photoelectron spectroscopic techniques.³⁸ All other four functionals underestimate the redox potential by more than 500 mV. Thus, the M06 functional is used throughout the computation of reduction potentials. It should be noted that we have also computed the redox potential of **1** with the larger basis set (def2-QZVP). We find that the computed potential is found to be -1.563 V that is similar to those we predicted with the def2-TZVP basis set. Thus, we have used the def2-TZVP basis set throughout.

Dedicated to Prof. Ponnambalam Venuvanalingam and Prof. Ian H. Hillier for their 70th and 80th birthdays.

■ ASSOCIATED CONTENT

SI Supporting Information

The Supporting Information is available free of charge at <https://pubs.acs.org/doi/10.1021/acsomega.3c01244>.

Optimized geometries of all species, computed LUMOs, binding energies of OTf⁻, functional dependence of LUMO with **1**, and optimized coordinates of all species (PDF)

■ AUTHOR INFORMATION

Corresponding Author

Mahesh Sundararajan – Theoretical Chemistry Section, Chemistry Division, Bhabha Atomic Research Centre, Mumbai 400 085, India; orcid.org/0000-0002-1522-124X; Phone: +91-22-2559 5607; Email: smahesh@barc.gov.in; Fax: +91-22-2559 5607

Complete contact information is available at:

<https://pubs.acs.org/doi/10.1021/acsomega.3c01244>

Notes

The author declares no competing financial interest.

■ ACKNOWLEDGMENTS

M.S. thanks BARC for computing facilities.

■ REFERENCES

- (1) Lovley, D. R.; Phillips, E. J. P.; Gorby, Y. A.; Landa, E. Microbial reduction of uranium. *Nature* **1991**, *350*, 413–416.
- (2) Suresh, A.; Subramaniam, S.; Srinivasan, T. G.; Rao, P. R. V. Studies on U-Th separation using tri-*sec*-butyl phosphate. *Solvent Extr. Ion Exch.* **1995**, *13*, 415–430.
- (3) Renshaw, J. C.; Butchins, L. J. C.; Livens, F. R.; May, I.; Charnock, J. M.; Lloyd, J. R. Bioreduction of uranium: environmental implications of a pentavalent intermediate. *Environ. Sci. Technol.* **2005**, *39*, 5657–5660.
- (4) Sundararajan, M.; Campbell, A. J.; Hillier, I. H. Catalytic Cycles for the Reduction of [UO₂]²⁺ by Cytochrome *c*₇ Proteins Proposed from DFT Calculation. *J. Phys. Chem. A* **2008**, *112*, 4451–4457.
- (5) Austin, J. P.; Sundararajan, M.; Vincent, M. A.; Hillier, I. H. The geometric structures, vibrational frequencies and redox properties of the actinyl coordination complexes ([AnO₂(L)_n]^m; An = U, Pu, Np; L = H₂O, Cl⁻, CO₃²⁻, CH₃CO₂⁻, OH⁻) in aqueous solution, studied by density functional theory methods. *Dalton Trans.* **2009**, *30*, 5902–5909.
- (6) Tsui, E.-Y.; Tran, R.; Yano, J.; Agapie, T. Redox-inactive metals modulate the reduction potential in heterometallic manganese-oxido clusters. *Nat. Chem.* **2013**, *5*, 293–299.
- (7) Kannan, S.; Barnes, C. L.; Duval, P. B. Versatile new uranyl(vi) dihalide complexes supported by tunable organic amide ligands. *Chem. Commun.* **2005**, *34*, 5997–5998.
- (8) Sather, A. C.; Berryman, O. B.; Rebek, J., Jr. Selective recognition and extraction of the uranyl ion from aqueous solutions with a recyclable chelating resin. *Chem. Sci.* **2013**, *4*, 3601–3605.
- (9) Das, C. P.; Roy, C.; Smiles, D. E.; Shuh, D. K.; Gronbeck-Jensen, M.; Prendergast, D.; Canning, A. Coordination Characteristics of Uranyl BBP Complexes: Insights from an Electronic Structure Analysis. *ACS Omega* **2017**, *2*, 1055–1062.
- (10) Penchoff, D. A.; Peterson, C. C.; Camden, J. P.; Bradshaw, J. A.; Auxier, J. D., II; Schweitzer, G. K.; Jenkins, D. M.; Harrison, R. J.; Hall, H. L. Structural Analysis of the Complexes of Uranyl, Neptunyl, Plutonyl and Americyl with Cyclic Imide Dioximes. *ACS Omega* **2018**, *3*, 13984–13993.
- (11) Bang, S.; Lee, Y.-M.; Hong, S.; Cho, K.-B.; Nishida, Y.; Seo, M.; Sarangi, R.; Fukuzumi, S.; Nam, W. Redox-inactive metal ions modulate the reactivity and oxygen release of mononuclear non-haem iron(III)-peroxo complexes. *Nat. Chem.* **2014**, *6*, 934–940.
- (12) Park, Y. J.; Ziller, J. W.; Borovik, A. S. The Effects of Redox-Inactive Metal Ions on the Activation of Dioxigen: Isolation and Characterization of a Heterobimetallic Complex Containing a Mn^{III}–(μ-OH)–Ca^{II} Core. *J. Am. Chem. Soc.* **2011**, *133*, 9258–9261.
- (13) Zegke, M.; Nichol, G. S.; Arnold, P. L.; Love, J. B. Catalytic one-electron reduction of uranyl(VI) to Group 1 uranyl(V) complexes via Al(III) coordination. *Chem. Commun.* **2015**, *51*, 5876–5879.
- (14) Periyasamy, G.; Sundararajan, M.; Hillier, I. H.; Burton, N. A.; McDouall, J. J. W. The binding of nitric oxide at the Cu (I) site of copper nitrite reductase and of inorganic models: DFT calculations of the energetics and EPR parameters of side-on and end-on structures. *Phys. Chem. Chem. Phys.* **2007**, *9*, 2498–2506.
- (15) Swart, M. A change in the oxidation state of iron: scandium is not innocent. *Chem. Commun.* **2013**, *49*, 6650–6652.
- (16) Krewald, V.; Neese, F.; Pantazis, D. A. Redox potential tuning by redox-inactive cations in nature's water oxidizing catalyst and synthetic analogues. *Phys. Chem. Chem. Phys.* **2016**, *18*, 10739–10750.
- (17) Hong, S.; Lee, Y.-M.; Sankaralingam, M.; Vardhaman, A. K.; Park, Y. J.; Cho, K.-B.; Ogura, T.; Sarangi, R.; Fukuzumi, S.; Nam, W. A Manganese(V)–Oxo Complex: Synthesis by Dioxigen Activation and Enhancement of Its Oxidizing Power by Binding Scandium Ion. *J. Am. Chem. Soc.* **2016**, *138*, 8523–8532.

- (18) Comba, P.; Lohr, A.-M.; Pfaff, F.; Ray, K. Redox Potentials of High-Valent Iron-, Cobalt-, and Nickel-Oxido Complexes: Evidence for Exchange Enhanced Reactivity. *Isr. J. Chem.* **2020**, *60*, 957–962.
- (19) Kumar, A.; Lionetti, D.; Day, V. W.; Blakemore, J. D. Redox-Inactive Metal Cations Modulate the Reduction Potential of the Uranyl Ion in Macrocyclic Complexes. *J. Am. Chem. Soc.* **2020**, *142*, 3032–3041.
- (20) Ghosh, T. K.; Mahapatra, P.; Drew, M. G. B.; Franconetti, A.; Fronera, A.; Ghosh, A. The Effect of Guest Metal Ions on the Reduction Potentials of Uranium(VI) Complexes: Experimental and Theoretical Investigations. *Chem. – Eur. J.* **2020**, *26*, 1612–1623.
- (21) Hay, P. J.; Martin, R. L.; Schreckenbach, G. Theoretical Studies of the Properties and Solution Chemistry of AnO_2^{2+} and AnO_2^+ Aquo Complexes for An = U, Np, and Pu. *J. Phys. Chem. A* **2000**, *104*, 6259–6270.
- (22) Shamov, G. A.; Schreckenbach, G. Density Functional Studies of Actinyl Aquo Complexes Studied Using Small-Core Effective Core Potentials and a Scalar Four-Component Relativistic Method. *J. Phys. Chem. A* **2005**, *109*, 10961–10974.
- (23) Bhattacharjee, S.; Isegawa, M.; Garcia-Rates, M.; Neese, F.; Pantazis, D. A. Ionization Energies and Redox Potentials of Hydrated Transition Metal Ions: Evaluation of Domain-Based Local Pair Natural Orbital Coupled Cluster Approaches. *J. Chem. Theory Comput.* **2022**, *18*, 1619–1632.
- (24) Matsui, T.; Kitagawa, Y.; Shigeta, Y.; Okumura, M. A Density Functional Theory Based Protocol to Compute the Redox Potential of Transition Metal Complex with the Correction of Pseudo-Counterion: General Theory and Applications. *J. Chem. Theory Comput.* **2013**, *9*, 2974–2980.
- (25) Austin, J. P.; Burton, N. A.; Hillier, I. H.; Sundararajan, M.; Vincent, M. A. Which density functional should be used to study actinyl complexes? *Phys. Chem. Chem. Phys.* **2009**, *11*, 1143–1145.
- (26) Arumugam, K.; Burton, N. A. Density functional theory (DFT) calculations of VI/V reduction potentials of uranyl coordination complexes in non-aqueous solutions. *Phys. Chem. Chem. Phys.* **2019**, *21*, 3227–3241.
- (27) Baik, M.-H.; Friesner, R. A. Computing redox potentials in solution: Density functional theory as a tool for rational design of redox agents. *J. Phys. Chem. A* **2002**, *106*, 7407–7412.
- (28) Kumar, A.; Lionetti, D.; Day, V. W.; Blakemore, J. D.; Kumar, A.; Lionetti, D.; Day, V. W.; Blakemore, J. D. *Chem. – Eur. J.* **2018**, *24*, 141–149.
- (29) Reath, A. H.; Ziller, J. W.; Tsay, C.; Ryan, A. J.; Yang, J. Y. Redox Potential and Electronic Structure Effects of Proximal Nonredox Active Cations in Cobalt Schiff Base Complexes. *Inorg. Chem.* **2017**, *56*, 3713–3718.
- (30) Calais, J.-L. Density-Functional Theory of Atoms and Molecules. *Int. J. Quantum Chem.* **1993**, *47*, 101.
- (31) TURBOMOLE V7.2, 2017, a development of University of Karlsruhe and Forschungszentrum Karlsruhe GmbH, 1989–2015, TURBOMOLE GmbH, since 2007, available from <http://www.turbomole.com>.
- (32) Becke, A. D. Density-Functional Exchange-Energy Approximation with Correct Asymptotic Behavior. *Phys. Rev. A: At., Mol., Opt. Phys.* **1988**, *38*, 3098–3100.
- (33) Becke, A. D.; Thermochemistry, D.-f. III. The Role of Exact Exchange. *J. Chem. Phys.* **1993**, *98*, 5648–5652.
- (34) Grimme, S.; Antony, J.; Ehrlich, S.; Krieg, H. A Consistent and Accurate Ab Initio Parametrization of Density Functional Dispersion Correction (DFT-D) for the 94 Elements H-Pu. *J. Chem. Phys.* **2010**, *132*, 154104.
- (35) Grimme, S.; Ehrlich, S.; Goerigk, L. Effect of Damping Function in Dispersion Corrected Density Functional Theory. *J. Comput. Chem.* **2011**, *32*, 1456–1465.
- (36) Weigend, F.; Ahlrichs, R. Balanced Basis Sets of Split Valence, Triple Zeta Valence and Quadruple Zeta Valence Quantity for H to Rn: Design and Assessment of Accuracy. *Phys. Chem. Chem. Phys.* **2005**, *7*, 3297–3305.
- (37) Sundararajan, M.; Sinha, V.; Bandyopadhyay, T.; Ghosh, S. K. Can Functionalized Cucurbituril bind Actinyl Cations Efficiently? A Density Functional Theory based Investigation. *J. Phys. Chem. A* **2012**, *116*, 4388–4395.
- (38) Khungar, B.; Roy, A.; Kumar, A.; Sadhu, B.; Sundararajan, M. Predicting the Redox Properties of Uranyl (VI/V) complexes using electronic structure calculations. *Int. J. Quantum Chem.* **2017**, *117*, No. e25370.
- (39) Pettersen, E. F.; Goddard, T. D.; Huang, C. C.; Couch, G. S.; Greenblatt, D. M.; Meng, E. C.; Ferrin, T. E. UCSF Chimera – A Visualization System for Exploratory Research and Analysis. *J. Comput. Chem.* **2004**, *25*, 1605–1612.
- (40) Hay, P. J.; Martin, R. L.; Schreckenbach, G. Theoretical Studies of the Properties and Solution Chemistry of AnO_2^{2+} and AnO_2^+ Aquo Complexes for An=U, Np and Pu. *J. Phys. Chem. A* **2000**, *104*, 6259–6270.